Version: Post-print

Publisher’s version: Sadeghian, Pedram; Fillmore, Brandon. 2018. Strain Distribution of Basalt FRP-Wrapped Concrete Cylinders. Case Studies in Construction Materials, 9. doi: https://doi.org/10.1016/j.cscm.2018.e00171

Strain Distribution of Basalt FRP-Wrapped Concrete Cylinders

Pedram Sadeghian[1] and Brandon Fillmore

Department of Civil and Resource Engineering, Dalhousie University, Halifax, NS, B3H 4R2, Canada.

ABSTRACT

This paper presents the results of an experimental study on the distribution of strain on a unidirectional basalt fiber-reinforced polymer (FRP) wrapped around concrete cylinders. A total of 12 cylinders (150 mm x 300 mm) were wrapped with 2, 4, and 6 layers of basalt FRP (BFRP) and the distribution of hoop strain under axial compression load was studied using multiple strain gauges. The new aspect of this study is the use of BFRPs as a new construction material for wrapping concrete elements with a focus on the distribution of hoop strain towards refining design strain of the wrap. Also, the effect of number of BFRP layers on the premature rupture of the wrap with respect to flat coupon test was evaluated in the form of a strain efficiency factor. It was concluded that the maximum hoop strain was not necessarily associated with the ruptured areas of the wrap. Also, an analysis of variances showed that the difference between hoop strains in the overlap and non-overlap regions was non-significant and an average hoop strain can represent the overall dilation of the specimens. The average strain efficiency factor was found ranging from 0.61 to 0.86. The test data was added to a large database of concrete cylinders wrapped with unidirectional FRPs and after statistical evaluations a refined strain efficiency factor of 0.70 was proposed instead of the current factor of 0.55 in ACI 440.2R-17 for design applications.

KEYWORDS: Strain efficiency; fiber-reinforced polymer; basalt; confinement; rupture.

https://doi.org/10.1016/j.cscm.2018.e00171

---

[1] Corresponding Author: Pedram.Sadeghian@dal.ca

1. INTRODUCTION

During the past three decades, the use of externally bonded fiber-reinforced polymer (FRP) composites for strengthening existing reinforced concrete (RC) columns have been extensively investigated [1][2][3][4][5]. Unidirectional FRP wraps made of carbon [6][7][8][9][10], glass [11][12][13], and aramid [14][15][16] have been typically applied in the circumferential (i.e. hoop) direction of circular cross-section of concrete specimens and tested under axial compression. Recently, basalt fibers have gained increasing attention as FRP materials for strengthening applications especially as an alternative to glass fibres (typically E-glass) [17][18][19].

Basalt is a natural, hard, dense, dark brown to black volcanic rock originating at a depth of hundreds of kilometers beneath the earth and reaching the surface as molten magma [20]. The current production technology for continuous basalt fibres is very similar to that used for E-glass fibers. The main difference is that E-glass is made from a complex batch of materials whereas basalt filament is made from melting basalt rock with no other additives. The simplicity of the manufacturing process reduces the production cost of basalt fibers [21]. As the production process does not require additives and a lower amount of energy is needed, it benefits in terms of environmental impact, economics, and plants' maintenance [22]. The quality and the chemical composition of the raw material have a major effect on cost and properties of basalt fibers and can lead to a broad range of fibres with different mechanical properties [22]. As a result, elastic modulus and strength of basalt FRP (BFRP) composites should be evaluated carefully.

Despite of numerous studies on concrete columns/cylinders wrapped with carbon, glass, and aramid FRP (CFRP, GFRP, and AFRP respectively), there is very limited experimental data on BFRP-wrapped concrete. In 2015, Sadeghian and Fam [24] collected a database containing 518 cylindrical concrete specimens confined with unidirectional FRPs and later the database was expanded to 774 specimens [22][23]. The database indicated that 68% of the specimens were confined with CFRP, 21% with GFRP, and 11% with AFRP composites. There was no study on unidirectional BFRPs at the time of the study. However, in 2011, Di Ludovico et al. [20] investigated the effectiveness of basalt fibers pre-impregnated with epoxy resin or latex and then bonded with a cement-based mortar (BRM) on concrete cylinders and compared the performance of the system with respect to GFRP wraps. In 2015, Campione et al. [19] studied a balanced bidirectional basalt fabric bonded with epoxy resin (BFRP) to concrete cylinders and tested the specimens under axial compression. The specimens confined with BFRP exhibited strain-softening behavior (after the peak load) with negligible increases in resistance but a significant increase in ultimate strain (up to 5 times the strain at peak load of unconfined concrete). It seems the bidirectional basalt fabric did not have enough stiffness providing minimum required lateral confinement pressure. Despite of the unpromising results, the authors of this paper believe that using unidirectional basalt fabric will provide enough lateral confinement for the concrete core and enhance the performance of the concrete.

Recently, Xie and Ozbakkaloglu [26] used unidirectional basalt fabric and made BFRP tubes filled with concrete made of recycled aggregates. Three and five layers of the unidirectional basalt fabric were used and the BFRP tube resulted in a strength gain for the concrete core. The tensile strength and modulus of BFRP coupons were obtained 1584 MPa and 76 GPa, respectively, calculated based on 0.14 mm nominal thickness of dry fabric. More recently, Ouyang et al. [27] presented a comparative study of the seismic behavior of square RC columns retrofitted with CFRP and BFRP sheets. The study demonstrated that the BFRP composites are expected to be a promising alternative to the conventional FRPs (e.g., CFRPs) for the seismic retrofit of square RC columns. The tensile strength and modulus of BFRP coupons were obtained 2048 MPa and 87

GPa, respectively, calculated based on 0.17 mm nominal thickness of dry fabric. Further studies were suggested to examine a wider range of FRP stiffness. As discussed, there are very limited studies in the literature on BFRP-confined concrete and there is a gap in the field to fill.

At the top of the lack of test data on BFRP-wrapped concrete, the concept of strain efficiency factor [28][29][30] of FRP wraps is still under investigation. Typically, the rupture of FRP in the hoop direction occurs at a strain level less than its rupture strain obtained from flat coupon tests [31][32][33][34][35][36]. The reduced rupture strain is required in most existing confinement models, usually in the form of a strain efficiency factor, as proposed by Pessiki et al. [29], which is the ratio of the reduced rupture strain of the FRP wrap to the rupture strain from flat coupon tests. Lam and Teng [37] calibrated the strain efficiency factor using 52 small-scale concrete cylinders wrapped with CFRPs and computed an average value of 0.59. Harries and Carey [32] computed a value of 0.58 for the strain efficiency factor using a database of 251 test results.

Bisby and Take [38] implemented an optical strain measurement technique and found the hoop strain is highly variable over the surface of an FRP-wrapped concrete cylinder and the coupon failure strain can be achieved, although only locally. It was shown that average strain efficiency factors varied between 0.77 and 0.80 for GFRPs and between 0.73 and 1.04 for CFRPs. Sadeghian and Fam [30] showed that strain efficiency factor varied significantly, from 0.12 to 1.22, with an average of 0.67 and a standard deviation of 0.23. The highly variable nature of the hoop strain was also reported by multiple studies [33][39][40]. Despite of numerous studies on parameters affecting the premature FRP rupture, ranging from geometrical discontinuity, triaxial stress states, geometrical imperfections, and non-uniform supports in test setup [28][33][41][42][43][44] there is no mechanics-based theory to consider synergy of all parameters affecting the strain efficiency of FRP-wrapped concrete. As the current strain efficiency factor of 0.55 in ACI 440.2R-17 [45] was proposed in early 2000 based on test data at the time, it is necessary to refine the design factor based on numerous new rest data since then and new materials such as BFRPs, which are the subject of this study.

This paper presents an experimental study on the distribution of hoop strain on concrete cylinders wrapped with unidirectional BFRPs. Three different number of BFRP layers, namely 2, 4, and 6 plies were considered and the specimens were instrumented with multiple strain and displacement gauges to capture axial and hoop strains developed during axial compression tests up to failure. The focus of the study is on the distribution of hoop strain using six strain gauges on the circumference of the wrap at the mid-height of the specimens. The results are compared to the rupture strain of flat coupons in the form of the strain efficiency factor and the significance of the strain variation is evaluated using an analysis of variances. At the end, the results are included in a large database of test data from the literature refining the strain efficiency factor for design applications.

2. EXPERIMENTAL PROGRAM

This section presents the details of test matrix, material properties, specimen preparation, test setup, and instrumentation of the test specimens.

2.1. Test Matrix

A total of 12 concrete cylinders with a diameter of 150 mm and a height of 300 mm were prepared. As shown in Table 1, the testing matrix included 4 groups of specimens, namely, plain (control), and wrapped with 2, 4, and 6 layers of BFRPs. Three identical specimens were prepared for each group. For wrapped specimens, a specimen identification (ID) system of LX was selected, where the first part “L” stands for layers and; and the second part “X” stands for the number of BFRP layers, namely 2, 4, and 6.

2.2. Material Properties

Concrete was delivered in a ready-mix batch with maximum aggregate size of 12.7 mm and slump of 100 mm. Due to limitation in the load capacity of the equipment available to the authors, the diameter of the specimens was limited to 150 mm and the maximum aggregate size of 12.7 mm was intentionally selected to be compatible with the size of the specimens. It should be noted that the scale effect is important and should be further studied. The tests on the plain concrete cylinders (150 x 300 mm) showed an average strength of 40.03 MPa (±1.97%) and average corresponding strain of 0.0029 mm/mm (±4.50%). The number in parentheses indicates the coefficient of variation (COV) of the corresponding parameter. The concrete was initially ordered to have a compressive strength of 25 MPa to be representative of a member to be retrofitted, however the ready-mix provider delivered higher strength. It should be highlighted that FRP wraps are more effective on low strength concrete than high strength one. If BFRPs are effective for the strength of about 40 MPa, they will be effective for low strength concrete too.

A unidirectional basalt fabric and epoxy resin were used for wrapping the specimens. For resin, a mixture of epoxy resin and slow hardener was used, which reported by manufacturer to have the tensile strength, tensile modulus, and maximum elongation of 50 MPa, 2.8 GPa, and 4.5%, respectively. The epoxy resin was reinforced by a unidirectional basalt fabric with the areal weight of 300 g/m^2. The tensile strength, tensile modulus, and rupture strain of basalt fibers were 2100 MPa, 105 GPa, and 2.6%, per manufacturer.

Five identical BFRP coupons made of two layers of the unidirectional fabric and epoxy resin were prepared using wet hand lay-up method and tested according to ASTM D3039 [46] in tension. A 100 kN universal testing machine with a displacement rate of 2 mm/min was used. A strain gauge was applied on each side of the coupons, centered in the longitudinal direction of fibers/coupon to measure the axial strain. Figure 1 shows the tensile test results of five identical coupons based on the nominal ply thickness of 0.23 mm. The average tensile strength and elastic modulus of BFRP coupons were obtained 1221.1 MPa (±2.75%) and 48.17 GPa (±0.32%), respectively. It should be highlighted that strain gauges broke at an average strain of 0.016 mm/mm. As the coupons were made of unidirectional fabric, the stress-strain curves were extended with the same modulus to the average tensile strength, which was resulted in the rupture strain of 0.0253 mm/mm. The linear behavior of the BFRP coupons and calculated rupture strain were further verified using the stroke calibrated with the strain gauge data. Implementation of a non-contact strain measurement method using either laser extensometer or digital image correlation (DIC) is recommended. It should be noted that the elastic modulus was calculated based on strain gauge readings.

2.3. Specimen Preparation

Cylindrical plastic molds with the inner diameter of 150 mm and height of 300 mm were used for the fabrication of concrete specimens. The fresh concrete was placed and consolidated in two layers using scoops, a vibration table, and then the surface was carefully troweled smooth. The consolidated concrete was left in the molds and covered to moist cure for 4 days before the molds were removed and the specimens were relocated to cure and get dry. After at least 28 days, the specimens were cleaned with a wire brush for wrapping procedure. The unidirectional basalt fabric was cut into to the length required for 2, 4, or 6 continuous layers plus a 150-mm overlap extension. The overlap was designed to cover a central angle of 120 degrees. The surface of each concrete specimen was cleaned of dust and covered with a coating of the epoxy resin using a roller. Then the fabric was gradually applied on the wet surface from one end and was saturated from the exterior surface as it was wrapped around the cylinder. After wrapping and saturating were complete, the surface was covered with a wax paper and any air pocket was removed usning a metal roller. After 7 days curing at ambient temperature, the wax paper was removed and the top and bottom ends of the specimens were strengthened with two layers of 25 mm wide straps of the same fabric. The straps were applied to prevent any premature failure due to stress concentration at the ends. After curing of the end straps, the specimens were capped with a Sulphur compound for uniform loading. Figure 2 shows some of the specimens after preparation.

2.4. Test Setup and Instrumentation

One specimen per each group of wrapped specimens were instrumented with six hoop strain gauges on the mid-height of the BFRP wrap with 60° central angle apart as shown in Figure 2. The first hoop strain gauge was installed at the middle of overlap region of the wrap (θ=0°) and then the second one at the end of overlap (θ=60°). The rest of hoop strain gauges were installed at 120°, 180° (middle of non-overlap region), 240°, and finally at 300° (the beginning of overlap region). The arrangement was specifically selected to obtain the distribution of hoop strain around the BFRP wrap on both overlap and non-overlap regions. The beginning and end of the overlap were targeted to capture any possible strain concentration due to discontinuity of the wrap. For other two specimens of each group, only two hoop strain gauges were installed at 90° and 270° angles. The specimens were also instrumented with two axial strain gauges, one on the middle of overlap region (0°) and another one on the middle of overlap region (180°) of the BFRP wrap. As shown in Figure 3, all specimens were instrumented with two displacement gauges along the axial direction of the specimen to measure average strain over 150 mm gauge length as a backup for the axial strain gauges. The plain specimens were instrumented with two lateral displacement gauges in the radial directions at 90° and 270° angles in addition to the axial ones. A 2 MN universal testing machine was used for testing with 0.6 mm/min displacement control loading rate. In addition to the strain and displacement gauges, the load and stroke were also collected by a data acquisition system at the rate of 10 data points per second.

3. TEST RESULTS AND DISCUSSION

This section presents the details of failure mode, effectiveness of BFRP wraps, stress-strain behavior, hoop strain distribution, strain efficiency factor, and refinement of strain efficiency factor for design applications.

3.1. Failure Mode

Figure 4 shows the specimens after failure. At the early stages of loading of the wrapped specimens, the noise related to the micro-cracking of concrete core was evident, indicating the start of stress transfer from the dilated concrete to the wrap. Prior to the failure, cracking noises were frequently heard. The failure pattern of BFRP-wrapped specimens was predominately due to hoop rupture of the wrap in the non-overlap region. For the specimens wrapped with two layers of BFRP (L2 specimens), the rupture of hoop fibers was gradually progressed up to a point that significant amount of the wrap was ruptured and the load dropped suddenly. With increasing the number of layers to four (L4) and six (L6) layers, the rupture of hoop fibers occurred in a shorter amount of time and the failure was more sudden with an explosive noise. Overall, the failure was controlled with rupture of the BFRP wrap in the non-overlap region around the mid-height of the specimens. Compared to the first author's previous observations on CFRP-wrapped cylinders [47], the failure of BFRP-wrapped cylinders was less explosive. This can be explained by lower modulus and strength of BFRPs than CFRPs and the fact that less energy was released at the time of failure. At the same time, the strength gain was significant as it is discussed in the following section.

3.2. Effectiveness of BFRP Wraps

The test results of BFRP-wrapped specimens are summarized in Table 2. The results show an average confined concrete strength (f'_{cc}) of 56.27 MPa (±0.79%), 76.98 MPa (±1.43%), and 94.57 MPa (±5.17%) for the specimens wrapped with 2, 4, and 6 layers of BFRPs, respectively. It indicates that wrapping concrete cylinders with 2, 4, and 6 layers of BFRP increased the compressive strength of plain concrete with a factor of 1.41, 1.92, and 2.36; respectively. Similarly, the results show an average confined concrete strain (ε_{cc}) of 0.0080 mm/mm (±5.22%), 0.0200 mm/mm (±3.03%), and 0.0238 mm/mm (±16.23%) for the specimens wrapped with 2, 4, and 6 layers of BFRPs, respectively. It means wrapping the plain concrete cylinders with 2, 4, and 6 layers of BFRPs increased the strain of plain concrete at peak load with a factor of 2.77, 6.95, and 8.25; respectively. As expected, FRP wrapping increased strain with higher rate than strength. It should be highlighted that only 4 layers of unidirectional basalt fabric with areal weight of 300 gsm/layer wrapped around a standard concrete cylinder with an epoxy resin almost doubled the strength of concrete. This indicates the effectiveness of BFRP composites for strengthening applications.

3.3. Stress-Strain Behavior

Figure 5 shows the stress–strain behavior of all specimens. Overall, the stress-strain curves of the wrapped specimens can be considered in three zones. In the first zone, the behavior of the wrapped concrete is mostly linear and similar to the plain concrete. In the second zone, as the concrete core dilates and the wrap is activated, the wrap is stretched and a tension stress in the wrap and a confinement stress on the concrete core are induced. In the third zone, because of large dilation, the wrap is fully activated and the confinement stress increases proportional to the stiffness of the wrap. The first and third zones are almost linear and the second zone is non-linear.

The axial strain on the right side of horizontal axis in Figure 5 was calculated based on average of two axial strain gauges installed on the BFRP wrap. The hoop strain on the left side of the horizontal axis was also calculated on average of all hoop strain gauges installed on the BFRP wrap. It should be noted that the axial strain of each specimen was also calculated from the axial displacement gauges and the results showed very good agreement with that of strain gauges. As the displacement gauges were bonded to the wrap using an adhesive and some of them were deboned before the ultimate load, the axial strains reported in this study are only based on the strain gauge data to be consistent for all specimens.

As shown in Figure 5, it can be observed that as the number of BFRP layers increases, the third zone slope increases to a point with higher stress and strain. However, the average hoop rupture strain does not increase. The distribution of hoop strain will be discussed more in depth in the following sections. Overall, all three identical specimens of each group resulted in almost identical stress-strain curve, which indicates the consistency of test results.

3.4. Volumetric Strain and Dilation

Figure 6 presents the variation of axial stress vs. volumetric strain of the specimens. The volumetric strain (ε_v) was calculated as follows:

$$\varepsilon_v = \varepsilon_a + 2\varepsilon_h \qquad (1)$$

where ε_a is the average axial strain and ε_h is the average hoop strain. As shown in the figure, the first zone of curves is linear and indicates an increasing negative volumetric strain (i.e. volume compaction) as axial stress increases. At a certain point, the behavior changes and volumetric strain starts to increase, which can be considered the beginning of the second zone (i.e. transition zone).

When volumetric strain becomes zero (i.e. volume of cylinder equals to initial volume), the third zone can be considered to begin. At this point the wrap is fully activated as the specimen enters to volume expansion. The specimens with 2 BFRP layers experienced a fast rate of volume expansion with a shallow third zone, which indicate the low stiffness of the wrap. As the number of BFRP layers increases, the slope of the third zone increases showing a significant gain of strength. In order to characterize the dilation properties of the specimens, dilation rate (μ) of each specimen can be calculated as follows:

$$\mu = \frac{\Delta\varepsilon_h}{\Delta\varepsilon_a} \tag{2}$$

where $\Delta\varepsilon_a$ is the change of average axial strain and $\Delta\varepsilon_h$ is the change of average hoop strain. The dilation rate was calculated based on the ratio of the slope of a line fitted into the axial strain for 10 adjacent data pints to that of the hoop strains rather than using only 2 adjacent data points to filter localized noises. Figure 7 shows the variation of dilation rate vs. axial strain of the specimens. Technically, the dilation rate is the Poisson's ratio of concrete at the first zone of stress-strain curve (i.e. linear behavior). Then, as the axial strain increases, the dilation rate increases almost exponentially. For plain specimens, the dilation rate approaches to infinity, which means crushing and spalling of concrete. For BFRP-wrapped specimen, the dilation rate reaches to a peak point and then decreases. It seems the axial strain corresponding the peak dilation rate corresponds to the strain of plain concrete at peak load. As the number of BFRP layers increases, the peak dilation rate decreases. As shown in Figure 7, the dilation rate of the specimens with 6 BFRP layers reaches a peak of about 1.25 and then decreases and stabilizes at an ultimate value of 0.5 which is Poisson's ratio of elastoplastic materials in the plastic region. The same trend can be seen for the specimens with 4 BFRP layers with a peak of about 1.75 and then an ultimate value of 1.0. The specimens with 2 BFRP layers show a peak dilation rate of about 4.0 and then it decreases to an ultimate value of about 2.0. The figure indicates that both peak and ultimate dilation rates depend on the number of BFRP layers (i.e. the wrap stiffness). Figure 8 shows the variation of hoop strain vs. axial strain of the specimens. All specimens exhibit an initial linear behavior with Poisson's ratio of about 0.2 and then with a nonlinear transition zone, the BFRP-wrapped specimens approach to a constant slope. The specimens wrapped with 4 and 6 BFRP layers approach to almost similar direction, but the specimens with 2 BFRP layers show a different direction. Overall, 4 and 6 layers of BFRP wraps were effective to control the dilation rate of concrete leading to a quasi-plastic behavior.

3.5. Hoop Strain Distribution

The focus of this paper is on the distribution of hoop strain on BFRP wrap. Figure 9 presents the variation of hoop strain vs. central angle at mid-height of the specimens as axial stress increases from a fraction of f'_{cc} to full f'_{cc}. The overlap region is also shaded in the figure. As shown in Figure 9(a), when the axial stress of specimen L2-1 is as low as 50 MPa (i.e. 0.89 f'_{cc}), the hoop strain has an almost uniform distribution. As axial stress increases, the hoop strain increase in a non-uniform pattern with a higher rate of increase in the non-overlap region. The non-uniform pattern with a peak at 180° (i.e. middle of non-overlap region) continues, until the wrap ruptures at the peak hoop strain of 0.0186 mm/mm, which is less than the rupture tensile strain of 0.0253 mm/mm corresponding to the flat coupon tests presented in Figure 1. Table 2 presents the peak strain comparing to the average of all strain gauges plus the average of strain gauges in the overlap and non-overlap regions.

Similarly, Figure 9 (b) and (c) present the variation of hoop strain for specimen L4-1 and L6-1, respectively. As shown, when the axial stress of the specimen is as low as 50 MPa (i.e. 0.65 f'_{cc} for L4-1 and 0.53 f'_{cc} for L4-1), the hoop strain has an almost uniform distribution. As axial stress increases, the hoop strain of L4-1 and L6-1 increase in a non-uniform pattern with a higher rate of increase in the non-overlap region. The non-uniform pattern with a peak at 240° and 180° (i.e. almost middle of non-overlap region) continues until the wrap ruptures at the peak hoop strain of 0.0211 and 0.0228 mm/mm, respectively, which is less than the rupture tensile strain of 0.0253 mm/mm. Overall, all specimens failed with a peak hoop strain around middle of non-overlap region lower than the rupture strain of flat coupon tests. However, as the number of BFRP layers increased, the peak hoop strain reached closer to the flat coupon rupture strain. Table 2 summarizes the average of all hoop strain gauges, peak hoop strain values, and the ratio of the peak over the average at the peak load of each BFRP-wrapped specimen. It indicates that the average ratio for specimen with 2, 4, and 6 layers of BFRPs is 1.12, 1.08, and 1.14; respectively.

Figure 10 shows the effect of number of BFRP layers on distribution of hoop strain at peak load comparing to the average hoop strain of specimen L2, L4, and L6. It seems the number of layer does not affect the overall strain distribution. In order to identify whether or not the number of BFRP layers had a significant effect on the strain distribution, an analysis of variance (ANOVA) was performed. ANOVA allows a comparison of the variance caused by the between-groups variability (mean square effect or MS_{effect}) with the within-group variability (mean square error or MS_{error}) by means of the F-test. The analysis results are presented in an F-value as follows:

$$F = \frac{MS_{effect}}{MS_{error}} \tag{3}$$

The ANOVA analysis tests whether the F-value is significantly greater than a critical value F_{crit}, extracted from the distribution of statistical tables based on the number of degrees of freedom. A test result (calculated from the null hypothesis and the sample) is called statistically significant if it is deemed unlikely to have occurred by chance, assuming the truth of the null hypothesis. A statistically significant result justifies the rejection of the null hypothesis. In this study, a one-way ANOVA using a confidence level of 95% (significance level of 0.05) was performed.

Considering the hoop strains recorded from six strain gauges of the first specimen of each group, the ANOVA analysis shows that the results are non-significant at the 5% significance level (F=2.59<F_{crit}=3.11), which accepts the null hypothesis, concluding that the variation of hoop strain of BFRP wraps around the concrete cylinders tested in this study is non-significant at the 5% significance level. In addition, the effect of number of BFRP layers on variation of hoop strain is also considered non-significant since F=1.15<F_{crit}=3.68. As a result, using the average hoop strain instead of peak hoop strain is justifies. To support further this conclusion, Figure 11 shows the ruptured areas of BFRP wraps compared with hoop strain distribution of the wraps at peak load. The figure indicates that the peak strain is not necessary in the ruptured area. It can be concluded that the variation of hoop strain is localized and is not associated with the ruptured areas of BFRP wraps considered in this study. Further study on other FRP materials is needed to generalize this conclusion.

3.5. Strain Efficiency Factor

In order to quantify the premature rupture of BFRP wraps with respect to flat coupon test result, the strain efficiency factor (κ_ε) of each specimen was calculated as follows:

$$\kappa_\varepsilon = \frac{\varepsilon_{h,rup}}{\varepsilon_{fu}} \tag{4}$$

where $\varepsilon_{h,rup}$ is the hoop strain in the FRP wrap at failure and ε_{fu} is the flat coupon's rupture strain in tension. Using the equation, the strain efficiency factor of each specimens was calculated and presented in Table 3. For comparison, the factor was calculated using both average hoop strain and peak hoop strain. The strain efficiency factor based on average hoop strain ranges from 0.61 to 0.86 with an average of 0.72 (±10.48%). The strain efficiency factor based on peak hoop strain ranges from 0.65 to 0.90 with an average of 0.78 (±10.78%). The ANOVA analysis shows that there is a non-significant difference between the strain efficiency factor based on average and peak hoop strains ($F=2.87<F_{crit}=4.49$). As a result, the strain efficiency factor based on average hoop strain can be used for further analyses of the specimens tested in this study. The ANOVA analysis also shows that there is a non-significant difference between the strain efficiency factor of the specimens wrapped with 2, 4, and 6 BFRP layers ($F=2.55<F_{crit}=5.14$). It means strain efficiency factor is not dependent on the thickness of the BFRP wrap. There is no in-depth study in the literature on the effect of FRP wrap thickness on strain efficiency factor. Thus, more research is needed using other FRP materials to generalize this conclusion.

3.6. Refining Design Strain Efficiency Factor

The concept of strain efficiency factor κ_ε has been implemented by the American Concrete Institute in ACI 440.2R-17 [45] which is the well-known guide for the design and construction of externally bonded FRP systems for strengthening concrete structures as follows:

$$\varepsilon_{fe} = \kappa_\varepsilon \varepsilon_{fu} \tag{5}$$

where ε_{fe} is the effective strain in FRP reinforcement attained at failure, ε_{fu} is the design rupture strain of FRP reinforcement, and κ_ε is equal to 0.55 per ACI 440.2R-17. The design guide offered some speculations on the reasons behind the reduction observed experimentally, including the multi-axial state of stress in the jacket, compared to the uniaxial state of stress in coupons. However, no rational approach was offered to express the hypothesis. Multiple studies have been performed to rationalize strain efficiency factor, however the complexity of the mechanics of the problem and the synergic effects of multiple parameters on the premature rupture of FRP wraps have made the problem too complicated to be solved completely. At this stage, the approach of ACI 440.2R-17 proposing a constant value based on experimental data seems more applicable for practicing engineers. The current design strain efficiency factor κ_ε of 0.55 was calibrated in early 2000 by Lam and Teng [37] and Harries and Carey [32] using 52 and 251 concrete cylinders wrapped with FRPs, respectively. As numerous test data has been produced in the past 15 years, a new calibration is necessary. In order to refine the factor, the test data of this study was added to the database collected previously [23] by combining two databases [24][25] to form a large database containing 783 concrete cylinders wrapped with unidirectional FRPs in the hoop direction resulting an average experimental strain efficiency factor of 0.70 with a standard deviation of 0.25. To evaluate the effect of the refinement, the FRP confinement model of ACI 440.2R-17 is used. The model was initially proposed by Lam and Teng [37] as follows:

$$\frac{f'_{cc}}{f'_{co}} = 1 + 3.3\frac{f_l}{f'_{co}} \tag{6}$$

where f'_{cc} is the confined concrete strength, f'_{co} is the unconfined concrete strength, and f_l is the confining stress defined as:

$$f_l = \frac{2E_f\varepsilon_{fe}t}{D} \tag{7}$$

where E_f is the elastic modulus of the FRP wrap in the hoop direction, t is the total thickness of the FRP wrap, D is the diameter of the concrete core, and ε_{fe} is the the effective strain defined in Eq. (5). The confinement model was used to predict the confined concrete strength as presented in Figure 12. Each circle in the figure represents the coordinate of a data point, where the horizontal axis is the experimental value and the vertical axis is the predicted value. It is noted that the fundamental approach to quantify the strain efficiency of FRP wraps is using the compressive constitutive law of FRP-confined concrete. As it was mentioned earlier, the analysis is complicated and beyond the scope of this study. The focus of the analytical section of this study is only calibrating the constant strain efficiency factor of ACI 440.2R-17 using its own confinement model.

To evaluate the performance of the refined factor, a statistical index known as Root Mean Square Error (RMSE) is implemented. RMSE is the square root of the variance of the residuals which is defined as the following, where n is the number of data points. RMSE indicates how close the predicted values (i.e., y) to the experimental values (i.e., x) as presented is the following equation. Lower values of RMSE indicate a better fit, with zero indicating a perfect prediction that means all data points are located on a 45-degree line.

$$RMSE = \sqrt{\frac{\sum(x-y)^2}{n}} \tag{8}$$

As shown in Figure 12, using the experimental strain efficiency factor, the confinement model can predict the experimental f'_{cc} to f'_{co} confining ratio with an RMSE of 0.318. However, using the strain efficiency factor of 0.55, the model underestimates the confining ratio with an RMSE of 0.481. Using the refined strain efficiency factor of 0.70, the data points get slightly closer to the 45-degree line indicating better prediction with an RMSE of 0.402. It means the dispersion degree is slightly enhanced, however there is no significant enhancement. The main point is that using the refined strain efficiency factor of 0.7 does not make the dispersion degree of data points worse than the factor of 0.55, however provides a better frequency distribution as it is discussed later in this section.

In addition to the RMSE index, the R^2 index (the square of the correlation coefficient) was computed for each case to evaluate the correlation between the predicted f'_{cc} and experimental f'_{cc}. As shown in Figure 12, the R^2 index between the predicted f'_{cc} and experimental f'_{cc} using the strain efficiency factor of 0.55 and 0.7 is the same (R^2=0.733) as changing the constant factor does not change the correlation between the predicted and experimental values. However, using a variable experimental strain efficiency factor, as expected, provides better correlation (R^2=0.836). It is important to note that a higher R^2 value does not necessarily indicate a perfect prediction. It only shows that there is a better linear correlation between predicted and experimental values. Thus, the R^2 index is not the best index for the evaluation presented in Figure 12, where RMSE is better suited. Figure 13 presents the variation of RMSE with respect to a range of strain efficiency factors. It clearly indicates that the proposed value of 0.70 for the strain efficiency factor corresponds to the minimum RMSE.

Figure 14 shows the frequency distribution of the ratio of predicted f'_{cc} to experimental f'_{cc}. Three strain efficiency factors based on the database (experimental κ_ε), ACI 440.2R-17 (κ_ε =0.55), and the refined factor (κ_ε =0.7). The histogram was prepared in 30 bins with the width of 0.04. The number of the bins was selected based on the square root of the number of the data points. The figure clearly indicates a better precision using the proposed strain efficiency factor of 0.70 in comparison with the ACI 440.2R-17 strain efficiency factor of 0.55.

It can be concluded that the strain efficiency factor in ACI 440.2R-17 can be changed from 0.55 to 0.70. It should be noted that this study focused on cylindrical cross-sections, the validity of the performed calibration in case of non-circular cross-sections needs to be tested. There are numerous statistical and analytical studies [48][49][50][51][52] in the literature to extend the analysis presented in this study. Also, a reliability analysis is needed to refine the strength reduction factors (i.e. phi factors) of the design guideline. Moreover, as new FRPs made of polyethylene terephthalate (PET) fibers [53][54], polyethylene naphthalate (PEN) fibers [54], and plant-based fibers [55] and bio-based resins [56] are emerging in the market, the strain efficiency factor needs to be studied more in-depth for new materials and revised accordingly.

4. CONCLUSION

This paper presented the results of an experimental study on concrete cylinders wrapped with unidirectional basalt fabrics (300 gsm). Three different number of basalt fiber-reinforced polymer (BFRP) layers, namely 2, 4, and 6 plies were considered and the specimens were instrumented with multiple strain gauges. The results were compared to the rupture strain of flat coupons in the form of a strain efficiency factor. The failure mode, strength gain, dilation, and variation of hoop strain of the specimens were also evaluated. The following conclusions can be drawn from the study:

- The failure of all specimens wrapped with BFRPs was controlled by the rupture of hoop fibers in the non-overlap region around the mid-height of the specimens. With increasing number of BFRP layers, the rupture of hoop fibers occurred in a shorter time window. In comparison with similar studies on CFRP, the failure of BFRP-wrapped cylinders was less explosive. This can be explained by lower modulus of BFRPs than CFRPs and the fact that less energy was released at the time of failure.
- Wrapping the plain concrete cylinders with 2, 4, and 6 layers of BFRPs increased the strength with a factor of 1.41, 1.92, and 2.36; respectively. This indicated the effectiveness of basalt fibers for concrete strengthening applications in addition to the other benefits in terms of environmental impact, economics, and plants' maintenance in comparison with fiberglass production.
- All specimens exhibited a dilation rate with an initial rate of about 0.2 and then with a nonlinear transition zone approaching to a constant rate. The specimens wrapped with 6 BFRP layers

approached to an average dilation rate of almost 0.5 indication the effectiveness of BFRP wraps to control dilation rate of concrete leading to a quasi-plastic behavior.

- Although the strain of the BFRP wraps in the hoop direction of the cylinders was variable, it was not associated with the ruptured areas of the wrap. An analysis of variances (ANOVA) on three specimens with six hoop strain gauges tested in this study showed that the variation is non-significant at 95% confidence level. In addition, the effect of number of BFRP layers on the variation of hoop strain amongst the three specimens was non-significant. More test results on strain distribution are needed to generalize this conclusion.
- The strain efficiency factor of the test specimens based on the average hoop strain ranged from 0.61 to 0.86 with an average of 0.72. The strain efficiency factor based on peak hoop strain ranged from 0.65 to 0.90 with an average of 0.78. An ANOVA analysis showed that there is a non-significant difference between the strain efficiency factor based on average and peak hoop strains. As a result, the strain efficiency factor based on average hoop strain was recommended for design applications.
- The test data of this study was added to a large database from the literature to form a database containing 783 concrete cylinders wrapped with unidirectional FRPs in the hoop direction resulting an average strain efficiency factor of 0.70 with a standard deviation of 0.25. The strain efficiency factor of 0.70 was proposed instead of the current factor of 0.55 in ACI 440.2R-17 design guideline predicting the strength of FRP-wrapped concrete cylinders in the database with the lowest statistical error. It should be noted that a reliability analysis will needed to refine the strength reduction factors (i.e. phi factors) of the design guideline.

5. ACKNOWLEDGEMENTS

The authors would like to acknowledge the financial support of NSERC and Dalhousie University.

6. CONFLICTS OF INTEREST

None.

7. REFERENCES

[1] Bakis C, Bank LC, Brown V, Cosenza E, Davalos JF, Lesko JJ, Machida A, Rizkalla SH, and Triantafillou TC. (2002). Fiber-reinforced polymer composites for construction-state-of-the-art review. Journal of Composites for Construction, 6(2), 73-87.

[2] Motavalli M, and Czaderski C. (2007). FRP composites for retrofitting of existing civil structures in Europe: state-of-the-art review. International Conference of Composites & Polycon., American Composites Manufacturers Association. Tampa, FL, USA.

[3] Hollaway LC. (2012). A review of the present and future utilisation of FRP composites in the civil infrastructure with reference to their important in-service properties. Construction and Building Materials, 24(12), 2419-45.

[4] Teng JG, Chen JF, Smith ST, and Lam L. (2003). Behaviour and strength of FRP-strengthened RC structures: a state-of-the-art review. Proceedings of the institution of civil engineers-structures and buildings, 156(1), 51-62.

[5] Nanni, A., and Bradford, N. M. (1995). FRP jacketed concrete under uniaxial compression. Construction and Building Materials, 9(2), 115-124.

[6] Xiao, Y., and Wu, H. (2000). Compressive behavior of concrete confined by carbon fiber composite jackets. Journal of materials in civil engineering, 12(2), 139-146.

[7] Lam, L., and Teng, J. G. (2004). Ultimate condition of fiber reinforced polymer-confined concrete. Journal of Composites for Construction, 8(6), 539-548.

[8] Berthet, J. F., Ferrier, E., and Hamelin, P. (2005). Compressive behavior of concrete externally confined by composite jackets. Part A: experimental study. Construction and Building Materials, 19(3), 223-232.

[9] Cui, C., and Sheikh, S. A. (2010). Experimental study of normal-and high-strength concrete confined with fiber-reinforced polymers. Journal of Composites for Construction, 14(5), 553-561.

[10] Micelli, F., and Modarelli, R. (2013). Experimental and analytical study on properties affecting the behaviour of FRP-confined concrete. Composites Part B: Engineering, 45(1), 1420-1431.

[11] Jiang, T., and Teng, J. G. (2007). Analysis-oriented stress–strain models for FRP–confined concrete. Engineering Structures, 29(11), 2968-2986.

[12] Almusallam, T. H. (2007). Behavior of normal and high-strength concrete cylinders confined with E-glass/epoxy composite laminates. Composites Part B: Engineering, 38(5), 629-639.

[13] Zohrevand, P., and Mirmiran, A. (2011). Behavior of ultrahigh-performance concrete confined by fiber-reinforced polymers. Journal of materials in civil engineering, 23(12), 1727-1734.

[14] Silva, M. A., and Rodrigues, C. C. (2006). Size and relative stiffness effects on compressive failure of concrete columns wrapped with glass FRP. Journal of Materials in Civil Engineering, 18(3), 334-342.

[15] Rochette, P., and Labossiere, P. (2000). Axial testing of rectangular column models confined with composites. Journal of composites for construction, 4(3), 129-136.

[16] Vincent, T., and Ozbakkaloglu, T. (2013). Influence of fiber orientation and specimen end condition on axial compressive behavior of FRP-confined concrete. Construction and Building materials, 47, 814-826.

[17] Sim, J., and Park, C. (2005). Characteristics of basalt fiber as a strengthening material for concrete structures. Composites Part B: Engineering, 36(6), 504-512.

[18] De Luca, A., Nardone, F., Matta, F., Nanni, A., Lignola, G. P., and Prota, A. (2010). Structural evaluation of full-scale FRP-confined reinforced concrete columns. Journal of Composites for Construction, 15(1), 112-123.

[19] Campione, G., La Mendola, L., Monaco, A., Valenza, A., and Fiore, V. (2015). Behavior in compression of concrete cylinders externally wrapped with basalt fibers. Composites Part B: Engineering, 69, 576-586.

[20] Di Ludovico, M., Prota, A., and Manfredi, G. (2010). Structural upgrade using basalt fibers for concrete confinement. Journal of composites for construction, 14(5), 541-552.

[21] Fiore, V., Di Bella, G. and Valenza, A., 2011. Glass–basalt/epoxy hybrid composites for marine applications. Materials & Design, 32(4), pp.2091-2099.

[22] Fiore, V., Scalici, T., Di Bella, G., and Valenza, A. (2015). A review on basalt fibre and its composites. Composites Part B: Engineering, 74, 74-94.

[23] Keshtegar, B., Sadeghian, P., Gholampour, A., and Ozbakkaloglu, T. (2017). Nonlinear modeling of ultimate strength and strain of FRP-confined concrete using chaos control method. Composite Structures, 163, 423-431.

[24] Sadeghian, P., and Fam, A. (2015). Improved design-oriented confinement models for FRP-wrapped concrete cylinders based on statistical analyses. Engineering Structures, 87, 162-182.

[25] Lim, J. C., & Ozbakkaloglu, T. (2014). Design model for FRP-confined normal-and high-strength concrete square and rectangular columns. Magazine of Concrete Research, 66(20), 1020-1035.

[26] Xie, T., and Ozbakkaloglu, T. (2016). Behavior of recycled aggregate concrete-filled basalt and carbon FRP tubes. Construction and Building Materials, 105, 132-143.

[27] Ouyang, L. J., Gao, W. Y., Zhen, B., and Lu, Z. D. (2017). Seismic retrofit of square reinforced concrete columns using basalt and carbon fiber-reinforced polymer sheets: A comparative study. Composite Structures, 162, 294-307.

[28] Chen, J. F., Li, S. Q., and Bisby, L. A. (2012). Factors affecting the ultimate condition of FRP-wrapped concrete columns. Journal of Composites for Construction, 17(1), 67-78.

[29] Pessiki, S., Harries, K. A., Kestner, J. T., Sause, R., and Ricles, J. M. (2001). Axial behavior of reinforced concrete columns confined with FRP jackets. Journal of Composites for Construction, 5(4), 237-245.

[30] Sadeghian, P., and Fam, A. (2014). A rational approach toward strain efficiency factor of fiber-reinforced polymer-wrapped concrete columns. ACI Structural Journal, 111(1), 135-144.

[31] Chen, J. F., Li, S. Q., Bisby, L. A., and Ai, J. (2011). FRP rupture strains in the split-disk test. Composites Part B, 42(4), 962–972.

[32] Harries, K. A., and Carey, S. A. (2003). Shape and “gap” effects on the behavior of variably confined concrete. Cement and Concrete Research, 33(6), 881-890.

[33] Smith, S. T., Kim, S. J., and Zhang, H. (2010). Behavior and effectiveness of FRP wrap in the confinement of large concrete cylinders. Journal of Composites for Construction, 14(5), 573–582.

[34] Bisby, L. A., Dent, A. J., and Green, M. F. (2005). Comparison of confinement models for fiber-reinforced polymer-wrapped concrete. ACI Structural Journal, 102(1), 62-72.

[35] De Lorenzis, L., and Tepfers, R. (2003). Comparative study of models on confinement of concrete cylinders with fiber-reinforced polymer composites. Journal of Composites for Construction. 7(3), 219-237.

[36] Xiao, Y., and Wu, H. (2000). Compressive behavior of concrete confined by carbon fiber composite jackets. Journal of Materials in Civil Engineering, 12(2), 139-146.

[37] Lam, L., and Teng, J. G. (2003). Design-oriented stress–strain model for FRP-confined concrete. Construction and building materials, 17(6), 471-489.

[38] Bisby, L. A., and Take, W. A. (2009). Strain localisations in FRP-confined concrete: new insights. Proceedings of the ICE-Structures and Buildings, 162(5), 301-309.

[39] Wu, Y. F., and Jiang, J. F. (2013). Effective strain of FRP for confined circular concrete columns. Composite Structures, 95, 479-491.

[40] El-Hacha, R., and Abdelrahman, K. (2013). Slenderness effect of circular concrete specimens confined with SFRP sheets. Composites Part B: Engineering, 44(1), 152-166.

[41] Vincent, T., and Ozbakkaloglu, T. (2015). Influence of overlap configuration on compressive behavior of CFRP-confined normal-and high-strength concrete. Materials and Structures, 1-24.

[42] Pham, T. M., Hadi, M. N., and Youssef, J. (2015). Optimized FRP Wrapping Schemes for Circular Concrete Columns under Axial Compression. Journal of Composites for Construction, 04015015.

[43] Fraldi, M., Nunziante, L., Carannante, F., Prota, A., Manfredi, G., and Cosenza, E. (2008). On the prediction of the collapse load of circular concrete columns confined by FRP. Engineering Structures, 30(11), 3247-3264.

[44] Lignola, G. P., Nardone, F., Prota, A., and Manfredi, G. (2012). Analytical model for the effective strain in FRP-wrapped circular RC columns. Composites Part B: Engineering, 43(8), 3208-3218.

[45] ACI 440.2R-17 (2017). “Guide for the design and construction of externally bonded FRP systems for strengthening concrete structures.” American Concrete Institute, Farmington, MI, USA.

[46] ASTM D3039 (2014). “Standard test method for tensile properties of polymer matrix composite materials.” Annual Book of ASTM Standards. West Conshohocken, PA, USA.

[47] Sadeghian, P., Rahai, A. R., and Ehsani, M. R. (2010). Effect of fiber orientation on compressive behavior of CFRP-confined concrete columns. Journal of Reinforced Plastics and Composites, 29(9), 1335-1346.

[48] Rousakis, T., Nistico, N., & Karabinis, A. (2012). Upgraded experimental database of uniformly FRP confined concrete columns for assessment of existing recommendations. In The 6th International Conference on FRP Composites in Civil Engineering–CICE (pp. 13-15).

[49] Yousif, D. S. T. (2013). New model of CFRP-confined circular concrete columns: ann approach. Int J Civil Eng Technol, 4, 98-110.

[50] Lim, J. C., Karakus, M., & Ozbakkaloglu, T. (2016). Evaluation of ultimate conditions of FRP-confined concrete columns using genetic programming. Computers & Structures, 162, 28-37.

[51] Cascardi, A., Micelli, F., & Aiello, M. A. (2017). An Artificial Neural Networks model for the prediction of the compressive strength of FRP-confined concrete circular columns. Engineering Structures, 140, 199-208.

[52] Mansouri, I., Kisi, O., Sadeghian, P., Lee, C. H., & Hu, J. W. (2017). Prediction of Ultimate Strain and Strength of FRP-Confined Concrete Cylinders Using Soft Computing Methods. Applied Sciences, 7(8), 751.

[53] Pimanmas, A., & Saleem, S. (2018). Dilation Characteristics of PET FRP–Confined Concrete. Journal of Composites for Construction, 22(3), 04018006.

[54] Dai, J. G., Bai, Y. L., & Teng, J. G. (2011). Behavior and modeling of concrete confined with FRP composites of large deformability. Journal of composites for construction, 15(6), 963-973.

[55] Wroblewski, L., Hristozov, D., & Sadeghian, P. (2016). Durability of bond between concrete beams and FRP composites made of flax and glass fibers. Construction and Building Materials, 126, 800-811.

[56] Mak, K., Fam, A., & MacDougall, C. (2015). Flexural behavior of sandwich panels with bio-FRP skins made of flax fibers and epoxidized pine-oil resin. Journal of Composites for Construction, 19(6), 04015005.

Table 1. Test matrix.

Group #	Group ID	Number of FRP layers	Number of identical specimens
1	Plain	0	3
2	L2	2	3
3	L4	4	3
4	L6	6	3
Total	-	-	12

Table 2. Summary of test results.

Specimen ID	Compressive strength f'_{cc} (MPa)	Ultimate axial strain ε_{cc} (mm/mm)	Average hoop strain at f'_{cc} (mm/mm)	Peak hoop strain at f'_{cc} (mm/mm)	Peak/ average strain ratio
L2-1	55.94	0.0084	0.0159	0.0186	1.17
L2-2	56.09	0.0079	0.0192	0.0222	1.16
L2-3	56.77	0.0076	0.0180	0.0184	1.02
L4-1	76.25	0.0195	0.0183	0.0222	1.21
L4-2	76.44	0.0207	0.0210	0.0213	1.02
L4-3	78.24	0.0199	0.0194	0.0198	1.02
L6-1	95.37	0.0232	0.0179	0.0228	1.27
L6-2	99.01	0.0279	0.0176	0.0178	1.01
L6-3	89.33	0.0202	0.0144	0.0166	1.15

Table 3. Comparison of average and peak strain efficiency factor.

Specimen ID	Average hoop strain (mm/mm)	Average κ_ε	Peak hoop strain (mm/mm)	Peak κ_ε
L2-1	0.0159	0.627	0.0186	0.736
L2-2	0.0193	0.761	0.0222	0.878
L2-3	0.0181	0.716	0.0184	0.729
L4-1	0.0184	0.728	0.0211	0.835
L4-2	0.0219	0.864	0.0213	0.841
L4-3	0.0194	0.769	0.0198	0.783
L6-1	0.0179	0.709	0.0228	0.901
L6-2	0.0176	0.698	0.0178	0.702
L6-3	0.0155	0.612	0.0166	0.655
Average		0.720		0.784

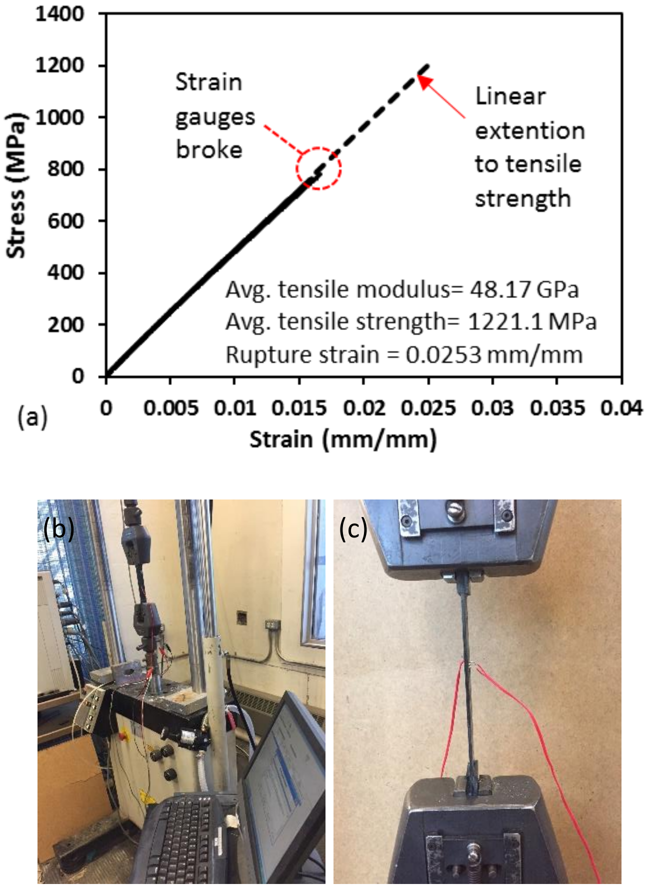

Figure 1. Material testing of BFRP coupons: (a) stress-strain behavior; (b) testing machine; and (c) strain gauged coupon.

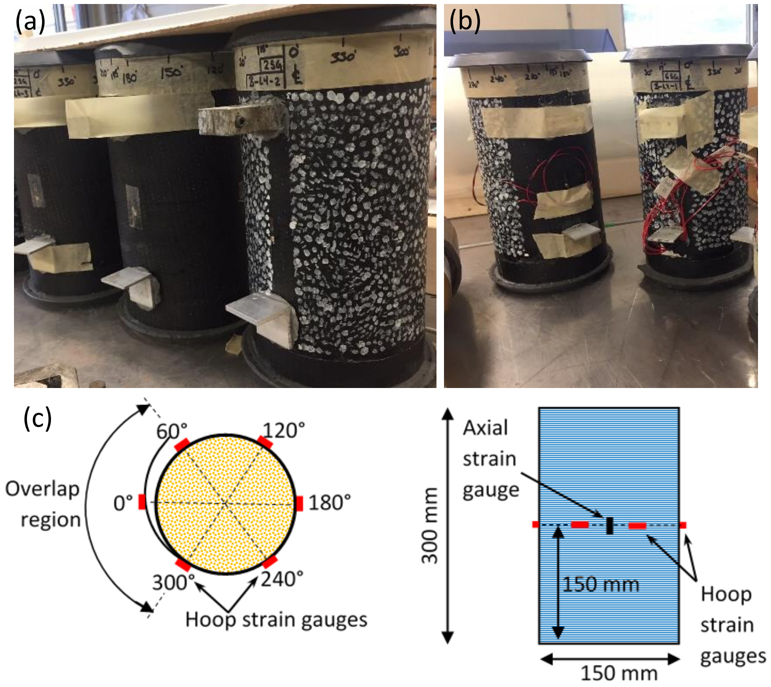

Figure 2. Specimen preparation and instrumentation: (a) bracket of displacement gauges applied; and (b) strain gauges weird; and (c) strain gauges arrangement.

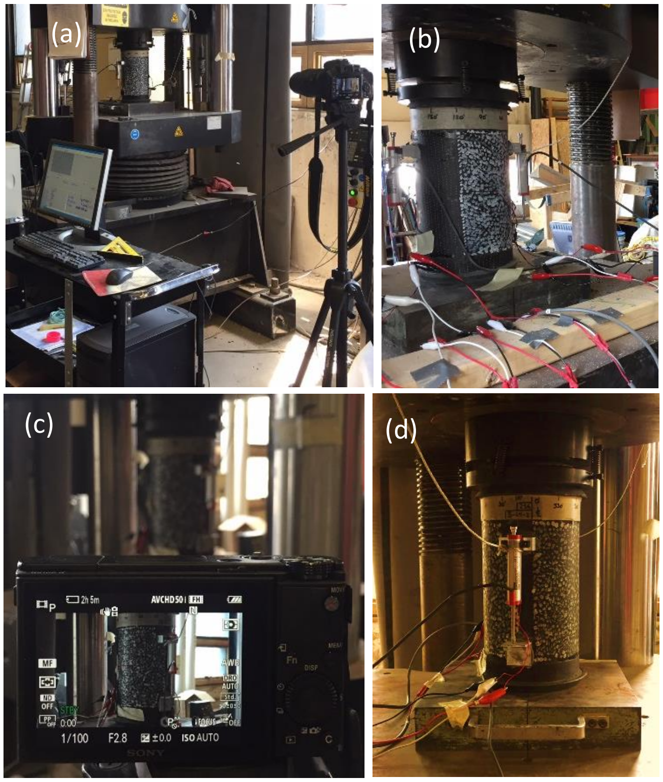

Figure 3. Test setup: (a) testing machine; (b) instrumentation; (c) camera; and (d) displacement gauge.

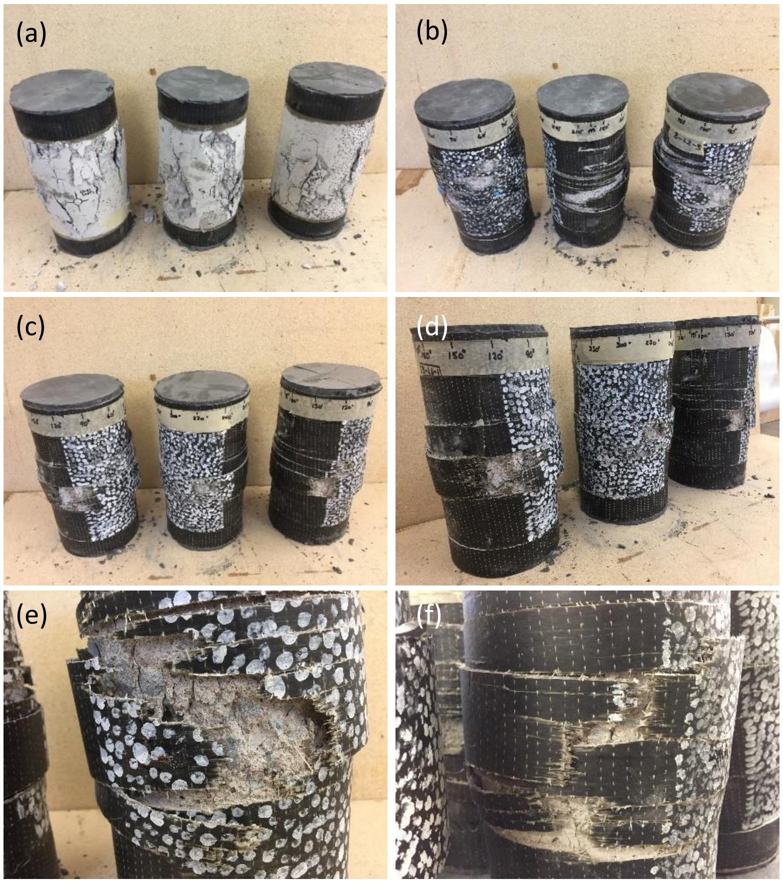

Figure 4. Test specimens after failure: (a) plain group; (b) L2 group; (c) L4 group; (d) L6 group; (e) and (f) typical rupture of hoop fibers.

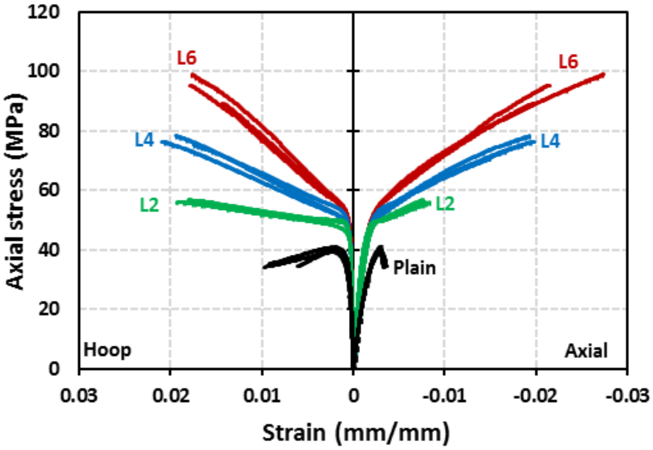

Figure 5. Stress-strain behavior of specimens.

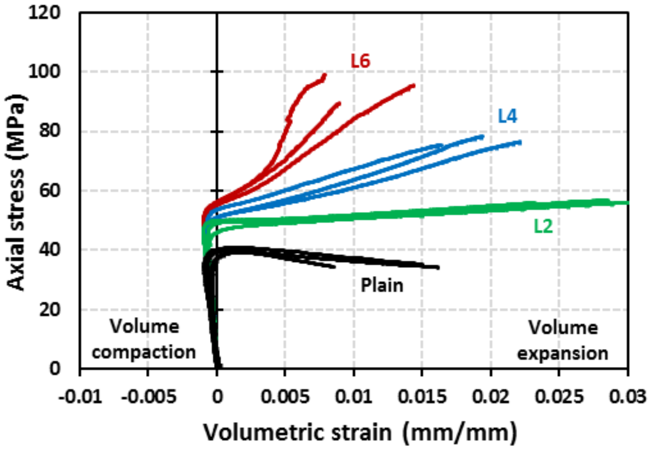

Figure 6. Variation of volumetric strain of specimens.

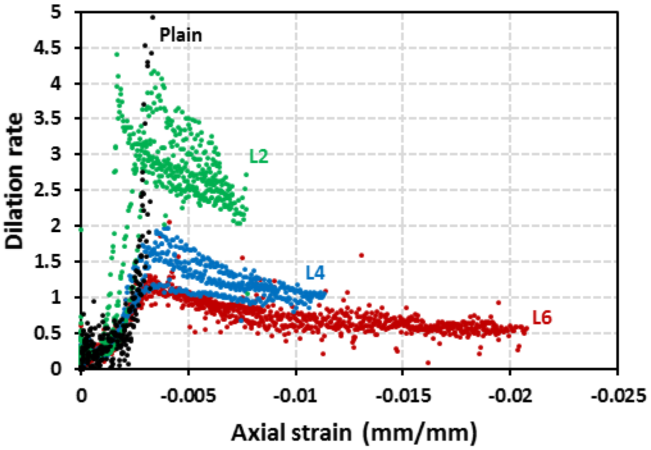

Figure 7. Variation of dilation rate vs. axial strain of specimens.

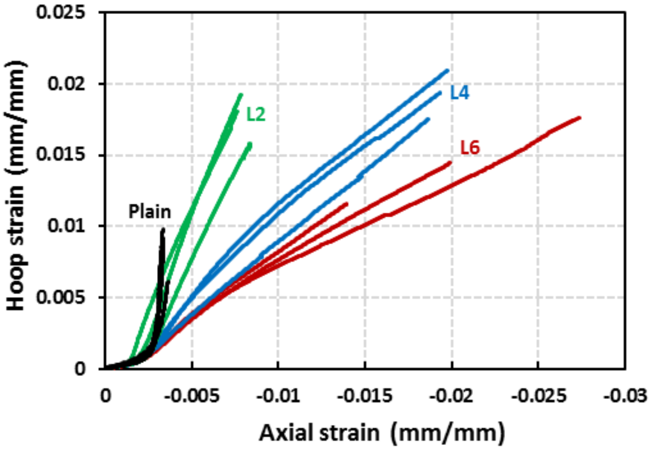

Figure 8. Variation of hoop strain vs. axial strain of specimens.

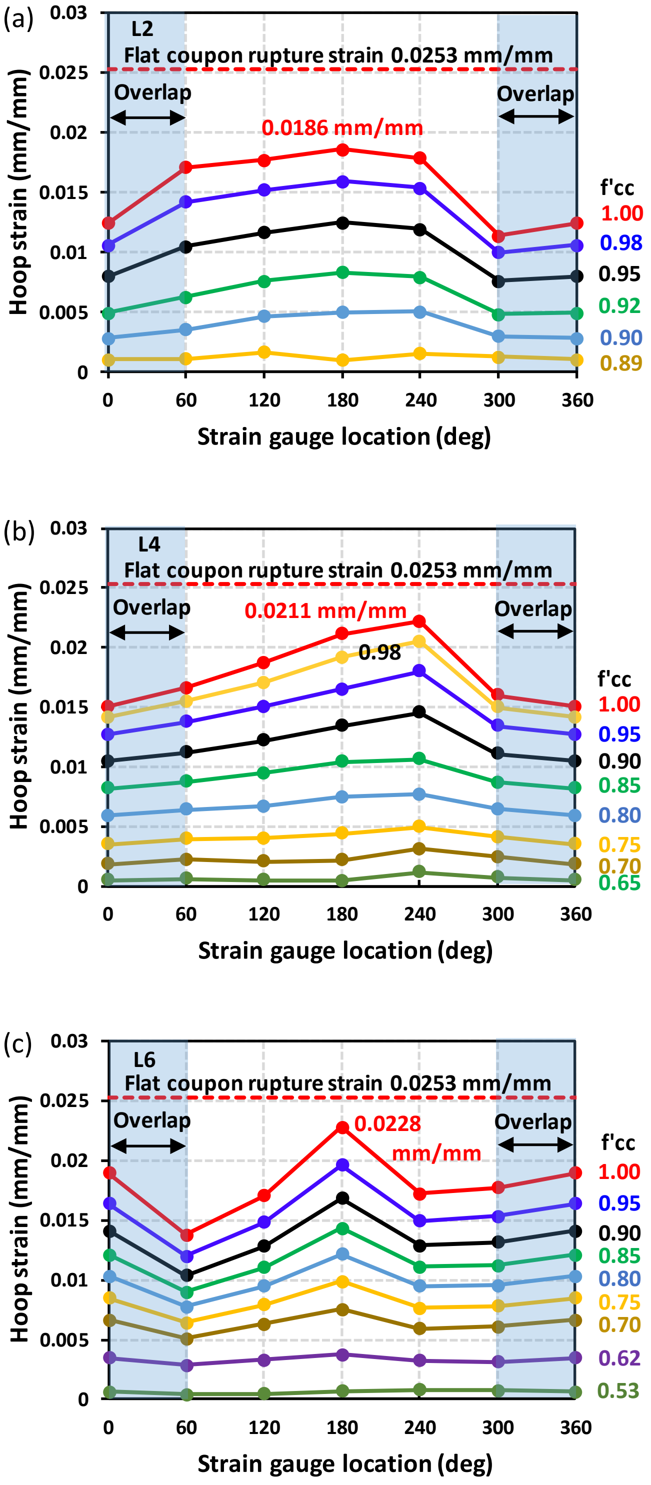

Figure 9. Distribution of hoop strain at mid-height of (a) L2, (b) L4, and (c) L6 specimens with six strain gauges.

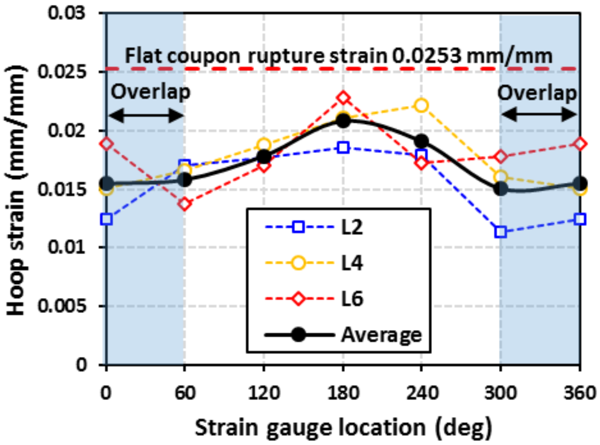

Figure 10. Effect of number of BFRP layers on distribution of hoop strain at peak load.

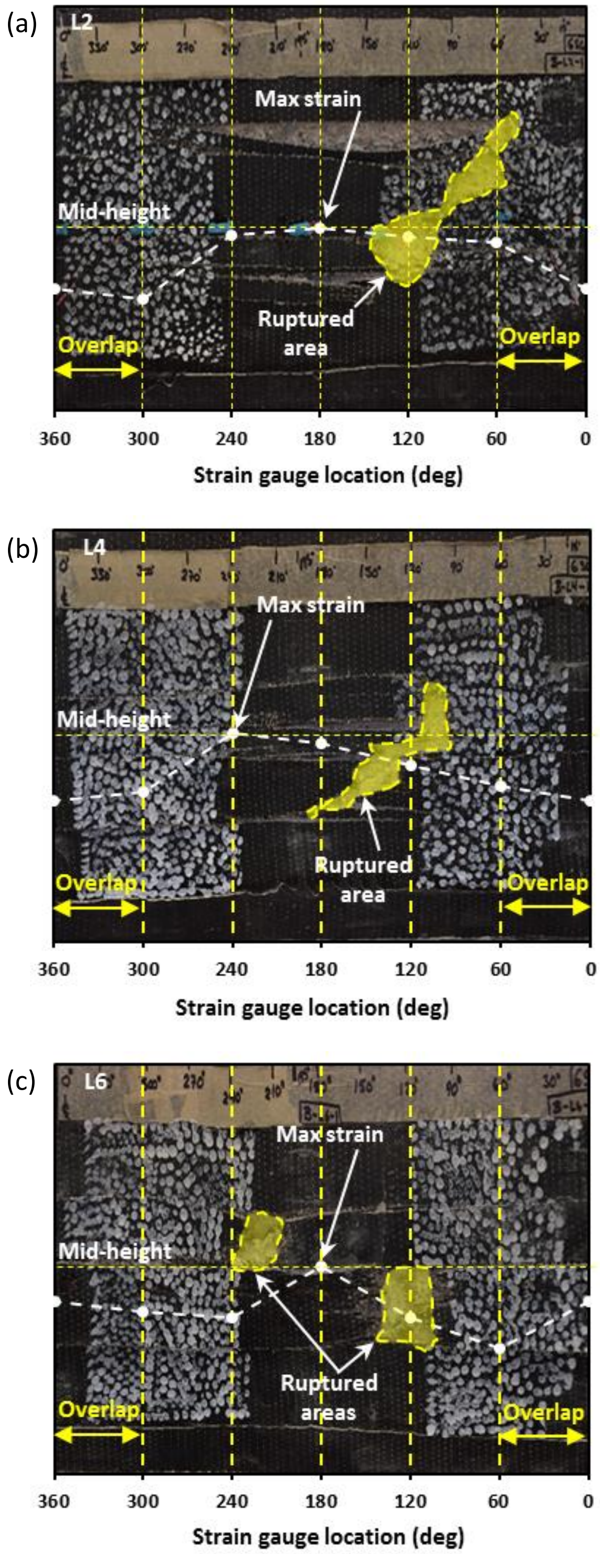

Figure 11. Ruptured areas of BFRP wrap compared with hoop strain distribution of (a) L2, (b) L4, and (c) L6 specimens with six strain gauges.

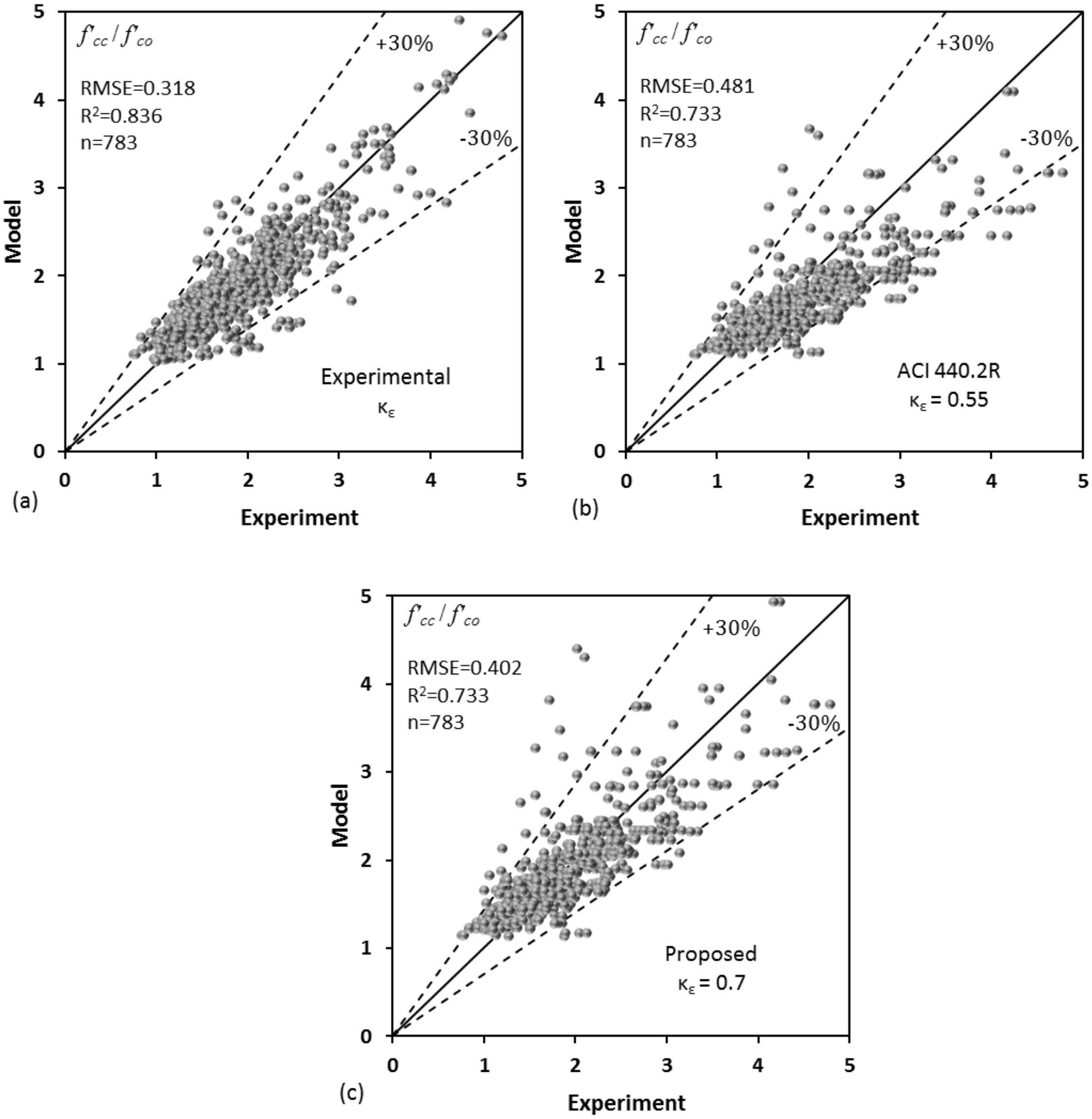

Figure 12. Performance of Lam and Teng [37] confinement model prediction f'_{cc}/f'_{co} using: (a) experimental strain efficiency factor; (b) ACI 440.2R-17 [45] strain efficiency factor of 0.55; and (c) refined strain efficiency factor of 0.70.

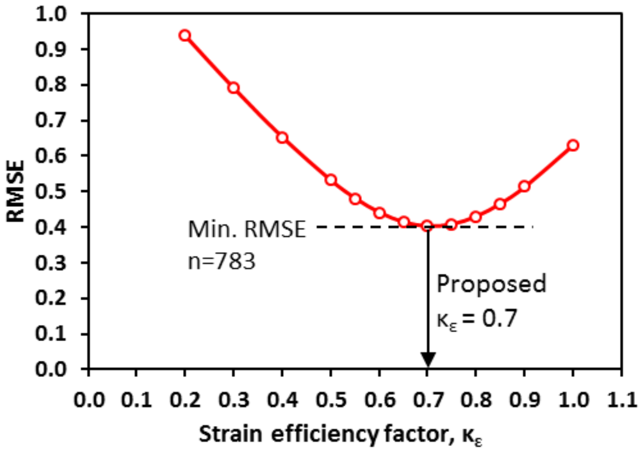

Figure 13. Calibration of a strain efficiency factor based on the performance of Lam and Teng [37] confinement model using 783 test data.

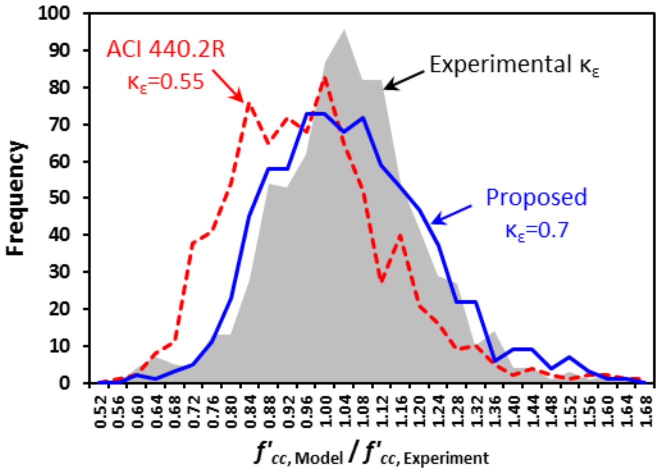

Figure 14. Frequency distribution of the *f'*$_{cc}$ (model) to *f'*$_{cc}$ (experiment) based on experimental, ACI 440.2R, and proposed strain efficiency factor using 783 test data.